Thermal Modeling of a Chip-Based Cold Atom Inertial Navigation System

Erich W. Brown[1]
Cosmiac at UNM, Albuquerque, New Mexico, 87106

Brent S. Taft[2] and 1Lt. Rachel Oliver[3]
U.S. Air Force Research Laboratory, Kirtland Air Force Base, New Mexico 87117

and

Kevin W. Irick[4]
Applied Technology Associates, Albuquerque, NM, 87123

Inertial Navigation Units (INUs) provide positioning data of an object when Global Positioning Systems are unable to do so. An anticipated main component of some future inertial navigation systems is a cold atom chip, that produces an electromagnetic field to corral atomic clouds into a viewing position. One challenge of chip integration is the high power requirement to generate the electromagnetic fields, resulting in large heat fluctuations which can interfere with the atomic cloud generation. A computational thermal model of the cold atom chip was developed to predict if more powerful chips can operate within thermal limits. Solution verification was performed using the Grid Convergence Index approach to evaluate model simulation results. The simulation results show that incorporation of an advanced thermal technology—namely an oscillating heat pipe—into the INUs allows for more power to be dissipated at a faster rate, resulting in the possibility of quicker and more precise navigation.

Nomenclature

A_c	=	Cross-Sectional Area, m^2
ATM	=	Advanced Thermal Management
GCI	=	Grid Convergence Index
GPS	=	Global Positioning System
g	=	Characteristic Function
H_h	=	Characteristic Mesh Size
h	=	Mesh number
I	=	Current, A
i	=	Index
INU	=	Inertial Navigation Unit
k	=	Thermal Conductivity, W/m·K
N_h	=	Total Number of Nodes
n	=	Total Number of Resistor Components
OHP	=	Oscillating Heat Pipe
P	=	Power, W

[1] Research Engineer, Cosmiac at UNM, 2350 Alamo Ave. SE, Ste. 300, Albuquerque, NM 87106, United States
[2] Senior Mechanical Engineer, U.S. Air Force Research Laboratory, Kirtland Air Force Base, NM 87117, United States
[3] Thermal Systems Engineer, U.S. Air Force Research Laboratory, Kirtland Air Force Base, NM 87117, United States
[4] Thermal Engineer, Applied Technology Associates, 1300 Britt St. SE, Albuquerque, NM 87123, United States

p	=	Apparent Order of Accuracy
q	=	Rate of Heat Transfer, W
R	=	Thermal Resistance, W/K
R_E	=	Electrical Resistance, Ω
R_{Eq}	=	Equivalent Resistance, W/K
r_{ij}	=	Mesh Ratio
s	=	Unit Direction Sign
SRQ	=	System Response Quantity
T	=	Temperature, K
T_x	=	Chip Temperature, K
$T_{x,ext}$	=	Extrapolated Chip Temperature, K
UA	=	Thermal Conductance, W/K
U_{num}	=	Numerical Uncertainty, K
V	=	Voltage, V
V_i	=	Volume of Node
y	=	Height, m
Δy	=	Change in Height, m
ε_a	=	Approximate Relative Error
ε_{ext}	=	Extrapolated Relative Error

I. Introduction

Global Positioning Systems (GPS) signals are vulnerable to physical obstructions, where, for example, they can be blocked by terrain or impeded due to jamming. In harsh environments, the GPS unit may no longer provide accurate navigation. Inertial Navigation Units (INUs) are being investigated for critical US Air Force missions as an alternative navigation method. Their fast and reliable information is needed in both terrestrial and extraterrestrial environments to prevent catastrophic mission failures. An INU that can provide navigation by using lasers and magnetic fields to generate atomic clouds is known as a cold atom INU. One shortcoming of a cold atom-based system is the time it takes to cool and collect the atoms for acceleration measurements. There are several contributing factors to this delay, but one of the main problems with the cycling rate is the amount of heat produced by the circuits on the chip [1,2].

The cold atom chip operates by using a laser to slow the momentum of the atoms that are released into a small vacuum chamber. The operating temperature of the chamber is maintained in the micro-Kelvin range, allowing the atoms to form a cloud that is sensed by a special camera. The cloud is used to determine the acceleration of the host vehicle. To get this cloud into the field of view, the circuits on the chip create a magnetic field that interacts with the cloud to corral it. If the cloud moves from the field of view, then the acceleration of the vessel is extrapolated from the rate of change and direction of movement.

The heat generated by powering the circuits radiates from the chips and interacts with the atomic cloud. It is possible that the energy absorbed by the atoms would be enough to excite them from their docile state and prevent cloud generation. Therefore, removing the heat generated by the circuits is critical for the increased performance of the INU. This can possibly be accomplished with advanced thermal technologies that are capable of handling more than 10 times the heat flux capacity of traditional thermal management solutions for similar critical systems.

Integration of advanced thermal management to a chip-based cold atom INU will produce more accurate and timely navigation. Modeling the cold atom chip—with and without advanced thermal technologies—is a cost-effective and an efficient way to demonstrate potential INU performance improvements. Thus, a thermal model for both configurations has been built in Thermal Desktop® for such an anlysis. A Grid Convergence Index (GCI) approach was used to verify the model so that simulation results can be used to provide insight into INU performance gains using integrated an advanced thermal management (ATM) technology.

II. Background

Extensive research has been performed over the last several years on cooling methods for high-power electronics. Traditionally, the maximum heat flux capacity that can be supported is 100 W/cm^2, which is 250 W/cm^2 less than the heat flux capacity of next-generation electronic processors. These new electronics are beneficial in many applications because they can be more efficient, require less space, and improve system capabilities.

Oscillating Heat Pipes (OHPs) and Annealed Pyrolytic Graphite Thermal Radiators are new thermal management technologies that can handle the heat flux capacity of the high-power electronics.

OHPs were first invented in 1987 [3] and have been researched heavily in the last few years [4-7] as demands for heat rejection have increased due to advances in high-power electronics. OHPs use passive forced convection through phase change to spread heat from an evaporator to a condenser—unlike traditional heat pipes that use latent heat transfer [9]. OHPs can be constructed out of many different materials and use any desired working fluid. Microchannels that are filled with the fluid create an anisotropic thermal conductivity in the longest legs of the microchannel. This means that the heat spreads quicker in the microchannel direction due to oscillations of liquid slugs and vapor plugs.

Another successful ATM technology is annealed pyrolytic graphite (APG). APG is a highly crystalline material that has thermal conductivity value that can be greater than 1500 W/m·K [8]. APG has proven especially effective for heat dissipation in thermally radiant environments as a thermal radiatior construction material. These passive thermal radiators are also compact and light weight, which saves money and reduces required space for implementation. Improvements of thermal efficiency and reduction of weight and size are all desired outcomes of the advanced thermal technologies.

III. System Description

A current test unit cold atom chip (see Figure 1) served as the basis for the chip thermal model development. Each chip is created by etching circuits into direct bonded copper substrates that serves as a facesheet to an aluminum nitride core. The bottom chip, shown in Figure 2a, is rectangular and has one circuit that runs across the bottom and another circuit across the top of the rectangular body. Together, this circuit is denoted as the X-Circuit and is designed to trap the atomic clouds in the viewing window. The top chip is a dog bone shape so that it does not interfere with the terminals of the bottom chip. The circuit is etched into the top of the chip and is routed in a U-Shape so that the magnetic fields corral the atoms. Figure 2b shows the schematic for the top chip. The chips are adhered to each other with Arctic Alumina® which improves the thermal conductance between the surfaces and serves as a dielectric to prevent circuit shorts. A temperature sensor was placed on the bottom side of the chip at the virtual intersection of the X-circuit.

Figure 1. Cold Atom Chip with Visible Circuits

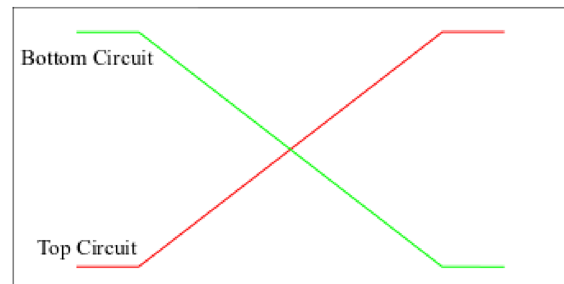

a)

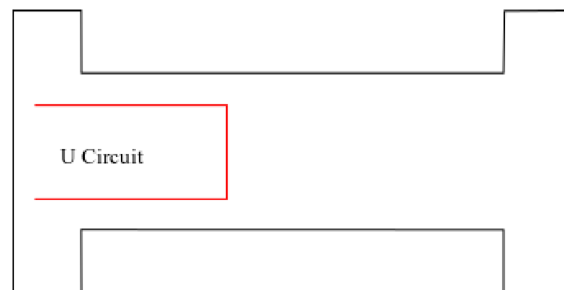

b)

Figure 2. Cold Atom Chip Schematic

IV. Thermal Model and Verification

Knowing the dimensions, boundary conditions, and operating parameters, each component of the cold atom chip was modeled to determine the temperature response for a given power input. Although most information provided was concrete, there were several estimated parameters that required sensitivity analyses. Thermal model solution verification was performed using the GCI, such as is used in [10], to present an estimate of simulation numerical uncertainty. Three meshes were used, showing grid convergence.

A. Model development

Incorporating all the parameters into the model is necessary for accuracy and adds uncertainty when information is unknown. Several factors for the model

were not known exactly, but a range was provided by experimentalists. This range allowed for studies to be performed to determine a temperature operation envelope. The thickness and thermal conductivity of the Arctic Alumina® and inclusion of natural convection needed to be investigated for their effects on the model.

1. Conductance Between Two Surfaces

When two bodies are placed against each other, heat transfers from the hot surface to the cold surface between the bodies. At this boundary, there is a typically a reduction of in effective thermal conductivity as compared to the thermal conductivity of the continuum media of the bodies. This reduction is due to micro-abrasions of the material which results in non-uniform surface connections. Thermal paste is used to improve the thermal conductance between the surfaces such as the Artic Alumina® used in this experiment. Thermal paste fills the micro-abrasions allowing for more uniform heat transfer from one surface to the other. The thermal conductivity of Artic Alumina® varies from 2 W/m·K to 12 W/m·K. The one-dimensional rate of heat transfer, q, is calculated by the thermal conductivity of the material, k, the cross-sectional area, A_c, perpendicular to heat flow, and the change in temperature, T, with respect to the distance, y, as shown in Equation (1).

$$q = -k \cdot A_c \cdot \frac{\partial T}{\partial y} \tag{1}$$

For the chip, the problem of heat transfer is simplified by assuming one-dimensional heat transfer from the bottom of the chip to the top because of the heat sink's position (located on the top surface of the top chip) and the thin thickness of the chip stack. Equation (1) can then be simplified to show the temperature gradient across the thickness of the insulation, shown in Equation (2), where T_i and y_i are the temperature and position of point i within a material.

$$q = -k \cdot A_c \cdot \frac{\Delta T}{\Delta y} = -k \cdot A_c \cdot \frac{T_2 - T_1}{y_2 - y_1} = k \cdot A_c \cdot \frac{T_1 - T_2}{y_2 - y_1} \tag{2}$$

Conductance, UA, between the surfaces can be calculated as follows:

$$UA = \frac{k \cdot A_c}{y_2 - y_1} \tag{3}$$

Thermal resistance, R, is inversely related to UA, as hown in Equation (4).

$$R = \frac{y_2 - y_1}{k \cdot A_c} = \frac{1}{\frac{k \cdot A_c}{y_2 - y_1}} = \frac{1}{UA} \tag{4}$$

Determining the R for each material is pivotal for understanding the heat flow parameters in the system. In the case of the cold atom chip, the thickness of the chips is significantly smaller than the length of the chip, so the heat may transfer through the thickness of the chip more easily than along the length of chip. Finding equivalent resistances through the thickness and along the length, by using one-dimensional resistance analysis, is completed by adding each resistance in series and in parallel, respectively. Figure 3 shows an example of how the resistances would look based on the chip configuration. The through-thickness resistances are computed by each material layer of the chip stack, and the lateral resistances represent the copper and aluminum nitride stack of a single chip. Equations (5) and (6) are used to determine the equivalent resistances, R_{Eq}, for series and parallel, respectively, where R_i is the thermal resistance of the ith component and n is the total number of components.

$$R_{Eq} = \sum_{i=1}^{n} R_i \tag{5}$$

$$\frac{1}{R_{Eq}} = \sum_{i=1}^{n} \frac{1}{R_i} \quad (6)$$

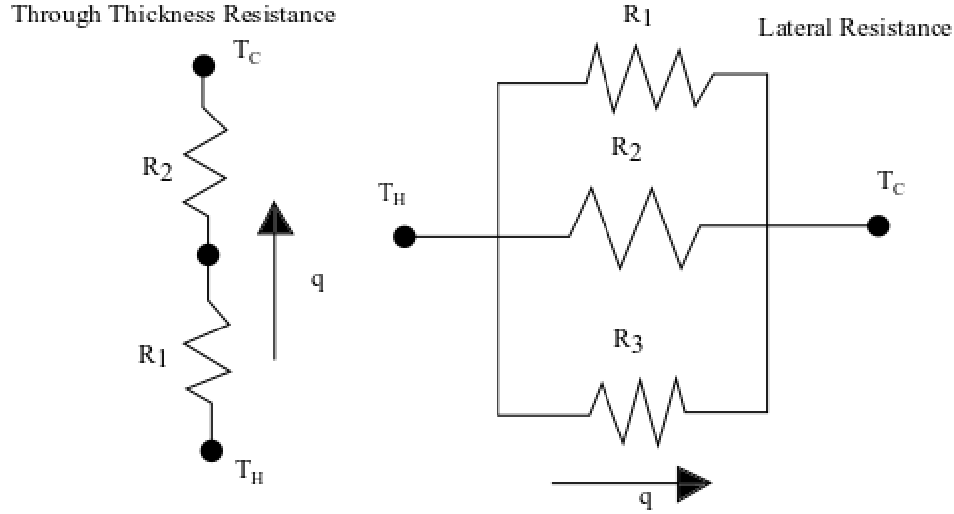

Figure 3. Thermal Resistance Example

2. Power

The power through the circuit, P, is the source of heat generation. This can be calculated with the voltage, V, current, I, and/or resistance, R_E. Equation (7) shows how power can be solved for by using V and I. Ohm's law allows for power to be solved using different variations of Equation (7) as shown in Equations (8) and (9).

$$P = V \cdot I \,. \quad (7)$$

$$V = I \cdot R_E \quad (8)$$

$$\therefore P = I \cdot R_E \cdot I = R_E \cdot I^2 \quad (9)$$

The system operates with a known steady current of 40 Amps at the power source. The X-Circuit's resistance was measured to be 0.14 Ω. Therefore, the instantaneous power is estimated to be 224.8 W. However, the power is pulsed during operation in 20-second periods, where power is on for 5 seconds and off for 15 seconds. An equivalent time-averaged constant power is 58.2 W. The uncertainty of the resistance measurement is ±0.03 Ω, and the current has an uncertainty of ±0.005 A, which will be accounted for later in the process.

B. Model Verification

The system response quantity (SRQ) in this investigation is the temperature, T_x, located at the center of the bottom-side of the bottom chip, essentially at the cross of the X-Circuit. The thermal model of an expected test apparatus was built in Thermal Desktop® using a combination of three-dimensional elements for the structural components, including the chip layers, thermal interface epoxies, and heat sink bar, with a stack-up shown in Table 1.

Table 2. Material Properties

Layer		Thickness (mm)	Material
Chip 1	1	0.127	Copper (incl. X-Circuit)
	2	0.625	Aluminum Nitride
	3	0.127	Copper (incl. X-Circuit)
	4	0.075	Thermal Adhesive
Chip 2	5	0.127	Copper
	6	0.625	Aluminum Nitride
	7	0.127	Copper
	8	0.075	Thermal Adhesive
	9	6.352	Cold Bar (fluid line & aluminum sink)

Essentially one-dimensional elements were used to model the path of the heater circuitry and to model the fluid loop driving the cold bar heat sink. Figure 4a through 4c show the three systematically-refined meshes used in this study for solution verification, where the mesh number, h, refers to the refinement of the mesh. Thus, h of 3 refers to the coarsest mesh, and h of 1 refers to the finest mesh.

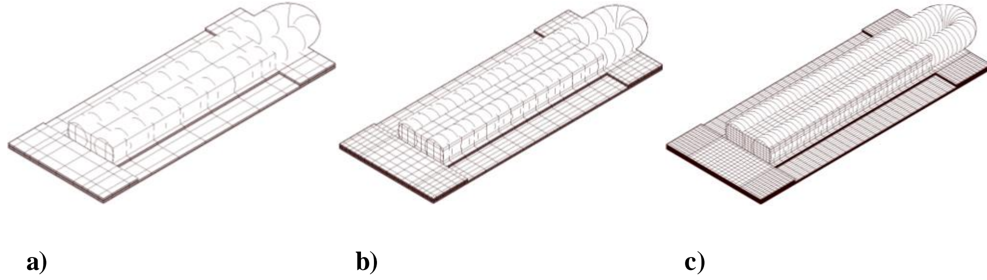

a) **b)** **c)**

Figure 4. Mesh Refinement

For this study, the characteristic mesh size, H_h, of mesh h is defined as

$$H_h = \left(\frac{\sum_{i=1}^{N_h} V_i}{N_h} \right)^{1/3} \tag{10}$$

where V_i is the volume of node i and N_h is the total number of nodes in mesh h. Likewise, r_{ij} is the ratio of meshes i and j, shown in the following equation, where mesh i is the coarser of the two meshes.

$$r_{ij} = \frac{H_i}{H_j} \tag{11}$$

Table 2 outlines the geometric properties of the meshes, where N_h is delineated for given element structure types.

The GCI is used in this work to define an approximation of numerical error, U_{num}, on T_x per [11], the application of which is described in [12,13]. This approach is executed by first computing the apparent order of accuracy, p, across the three meshes, as shown in Equation 12.

Table 3. Model Geometry Parameters

h	N_h			H_h	r_{ij}
	Solids	**Heater Lines**	**Pipe Line**		
3	716	34	27	0.00290	---
2	8968	64	52	0.00130	2.32
1	86936	124	102	0.00059	2.13

$$p = \frac{\left| \ln \left| \frac{(T_{x,3} - T_{x,2})}{(T_{x,2} - T_{x,1})} \right| + g(p) \right|}{\ln \left(\frac{H_2}{H_1} \right)} \qquad (12)$$

In this case, g, is a characteristic function computed simultaneously (or iteratively) with p, as follows:

$$g(p) = \ln \left(\left((H_2/H_1)^p - s \right) \Big/ \left((H_3/H_2)^p - s \right) \right) \qquad (13)$$

Here, s is made to be

$$s = sign \left(\frac{\left(T_{x,3} - T_{x,2} \right)}{\left(T_{x,2} - T_{x,1} \right)} \right) \qquad (14)$$

An approximate relative error, ε_a, can be defined between meshes 1 and 2 as

$$\varepsilon_a = \left| \frac{\left(T_{x,1} - T_{x,2} \right)}{T_{x,1}} \right| \qquad (15)$$

The fine GCI is found by

$$GCI = \frac{1.25 \cdot \varepsilon_a}{\left(\left(\frac{H_2}{H_1} \right)^p - 1 \right)} \qquad (16)$$

where the 1.25 is a safety factor given by the fact that p is greater than or equal to the second-order formal order of accuracy reported in the documentation for Thermal Desktop® [14]. An extrapolated SRQ, $T_{x,ext}$, and an associated extrapolated relative error, $\varepsilon_{a,ext}$, can be computed with the following two equations:

$$T_{x,ext} = \frac{\left(\left(\frac{H_2}{H_1} \right)^p T_{x,1} - T_{x,2} \right)}{\left(\left(\frac{H_2}{H_1} \right)^p - 1 \right)} \qquad (17)$$

$$\varepsilon_{ext} = \left| \frac{\left(T_{x,ext} - T_{x,1} \right)}{T_{x,ext}} \right| \qquad (18)$$

From this GCI describe above, U_{num} can bed approximated as

$$U_{num} = GCI \cdot T_{x,1} \tag{19}$$

V. Model Results

A. Simulation Results

Figures 5a through 5h show a sample set of temperature contour plots for the 67.488 W case. The top row shows the temperature distribution for the copper configuration, and the bottom shows temperature for the ATM configuration which assumes 1000 W/m-K thermal conductivity along the length of the chips (as opposed to 410 W/m-K for the standard chip). The images show a bottom view of the chip set for meshes 3 through 1 (left to right) and an isometric view of the entire model for the finest mesh at the far right. Figure 6 shows the grid convergence of the copper and ATM solutions, where Tables 3 and 4 show the sensitivity study and verification parameters for the effects of P on T_x.

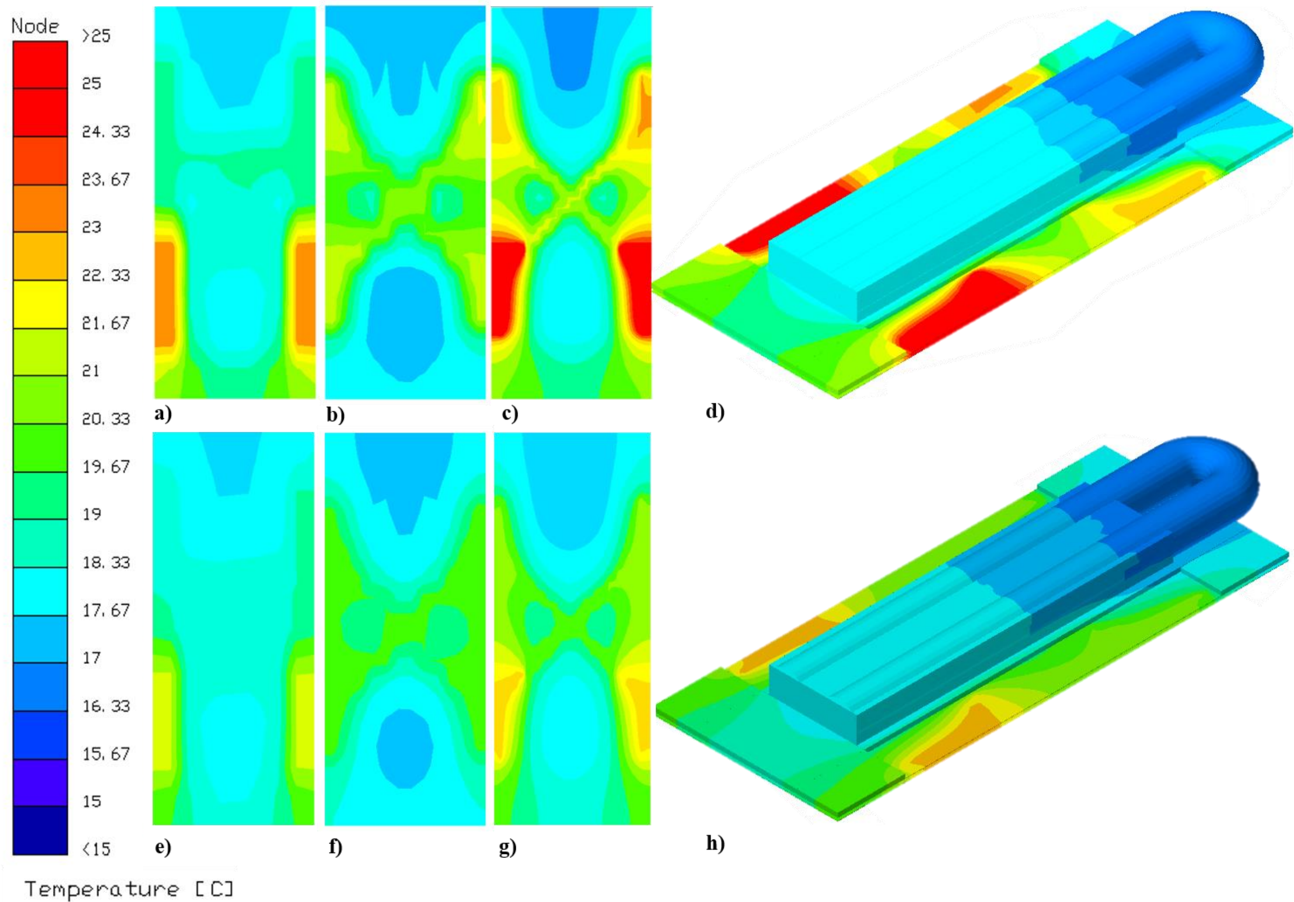

Figure 5. Temperature Contour Plots

Finally, Figure 7 plots the T_x results against P for both copper and ATM configurations, where the error bars correspond to U_{num}. The power applied to the model is averaged over 20 seconds, where 225 W is applied for 5 seconds and then the chip can cool for 15 seconds. Simplifying the system this way enabled sensitivity studies to be conducted for the model.

One-at-a-time model sensitivity studies for the varying parameters of Arctic Alumina® was investigated, which included thermal conductivity and layer thickness. Difficulties in the manufacturing process of the thermal paste creates a range of possible thermal conductivity values from 2 W/m-K to 12 W/m-K, Figures 8 shows the results of this study. To minimize the thermal resistance of the Arctic Alumina® layer, the thermal paste thickness must also be minimized during the manufacturing process. However, the exact thickness is difficult to measure. A sensitivity

study examined the possible range of thicknesses between 0.075 mm and 0.1 mm that was provided by the primary experimentalists who constructed the chip. The range of possible temperatures due to the uncertainty in this variable are shown in Figure 9.

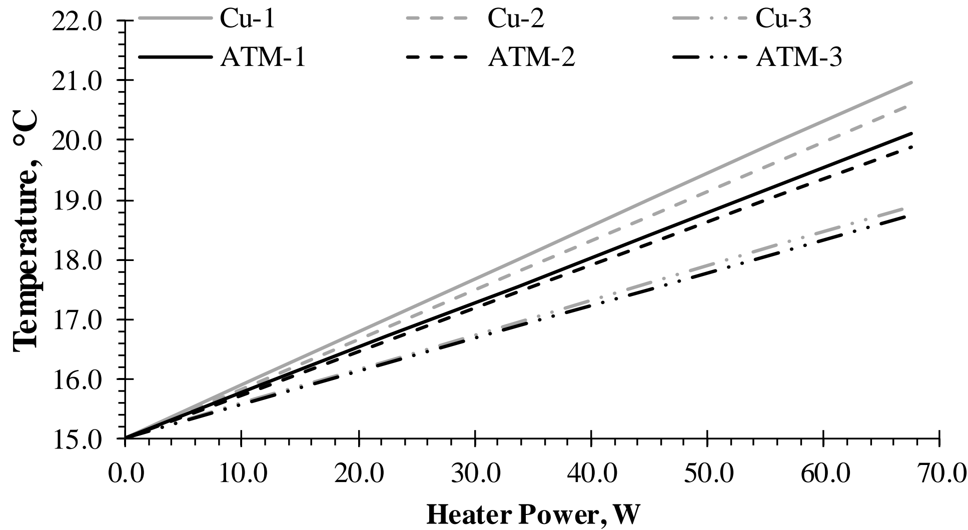

Figure 6. Mesh Convergence Study

Table 4. Sensitivity Study on Model without ATM

P	Tx	Tx,ext	p	ε_a	ε_{ext}	GCI	Unum
11.248	16.00	16.03	1.66	0.0041	0.0016	0.20%	0.033
22.496	17.00	17.05	1.66	0.0078	0.0031	0.38%	0.065
33.744	18.00	18.08	1.66	0.0110	0.0043	0.54%	0.098
44.992	18.99	19.10	1.67	0.0139	0.0055	0.69%	0.130
56.24	19.99	20.12	1.67	0.0165	0.0065	0.81%	0.163
67.488	20.98	21.13	1.67	0.0188	0.0074	0.93%	0.195

Table 4. Sensitivity Study on Model with ATM

P	Tx	Tx,ext	p	ε_a	ε_{ext}	GCI	Unum
11.248	15.86	15.87	1.88	0.0024	0.0007	0.09%	0.015
22.496	16.71	16.73	1.88	0.0045	0.0014	0.18%	0.029
33.744	17.56	17.60	1.88	0.0064	0.0020	0.25%	0.044
44.992	18.41	18.46	1.88	0.0081	0.0025	0.32%	0.059
56.24	19.26	19.32	1.89	0.0096	0.0030	0.38%	0.073
67.488	20.10	20.17	1.89	0.0111	0.0035	0.44%	0.088

Under normal testing conditions, the cold atom chip is exposed to ambient temperatures and therefore subject to natural convection. The temperature in the room is measured at 23.33 °C (74 °F). Figure 10 shows the results of the model when natural convection is accounted for. The rise in temperature, as seen when the power is 10 to 20 W in Figure 10, is due to the room being warmer than the initial temperature of the chip. As the power input increases the difference in temperature starts to decrease because natural convection begins to remove heat.

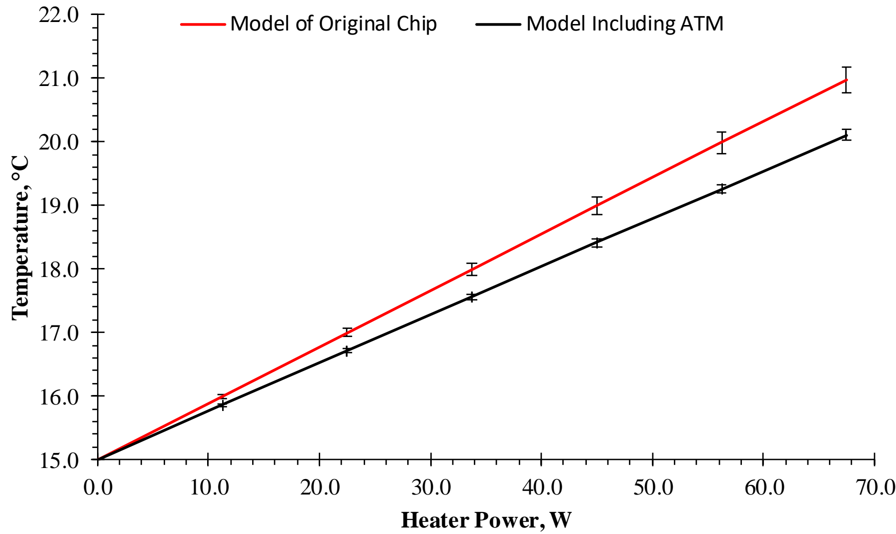

Figure 7. Temperature vs. Power Results

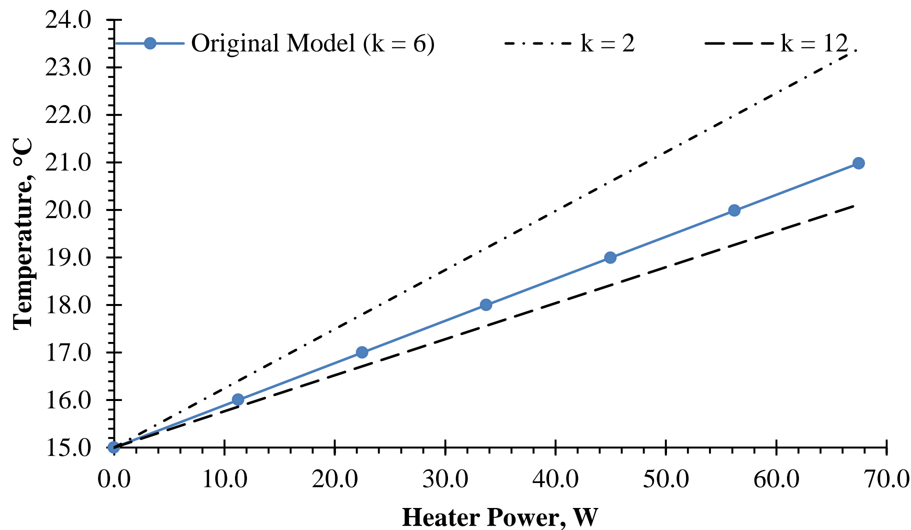

Figure 8. Thermal Conductivity Sensitivity Study

These sensitivity studies show that the model acts as it physically should, such as if the thermal conductivity increases then the maximum temperature decreases. Combining all the parameters that reduced the temperature in a cold case results in a lower possible operating temperature range. Similarly, the parameters that increased the temperature were combined to create the upper operating range. Figure 10 shows the operating envelope, due to the unknown system quantities. Due to the uncertainty of the parameters, this operating range cannot be refined any further and actual measurements should fall within the envelope.

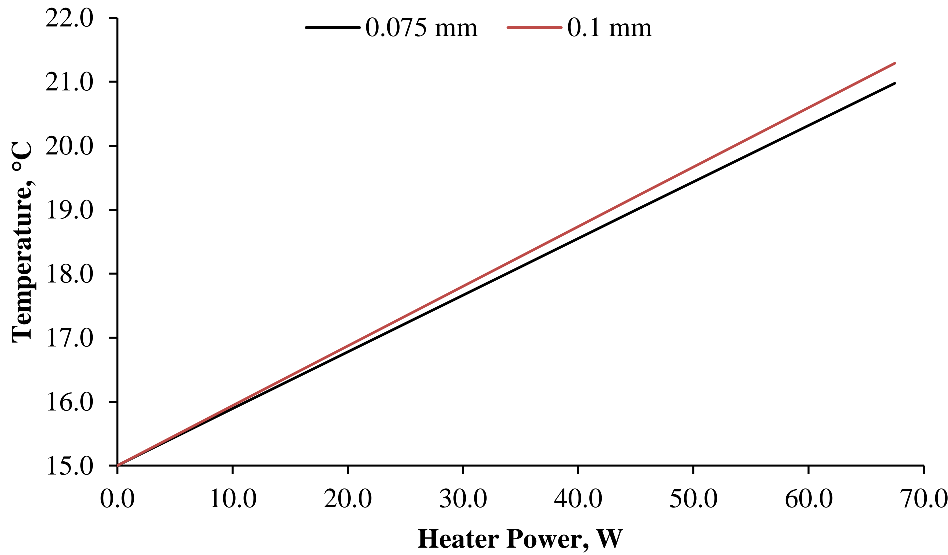

Figure 9. Thickness Sensitivity Study

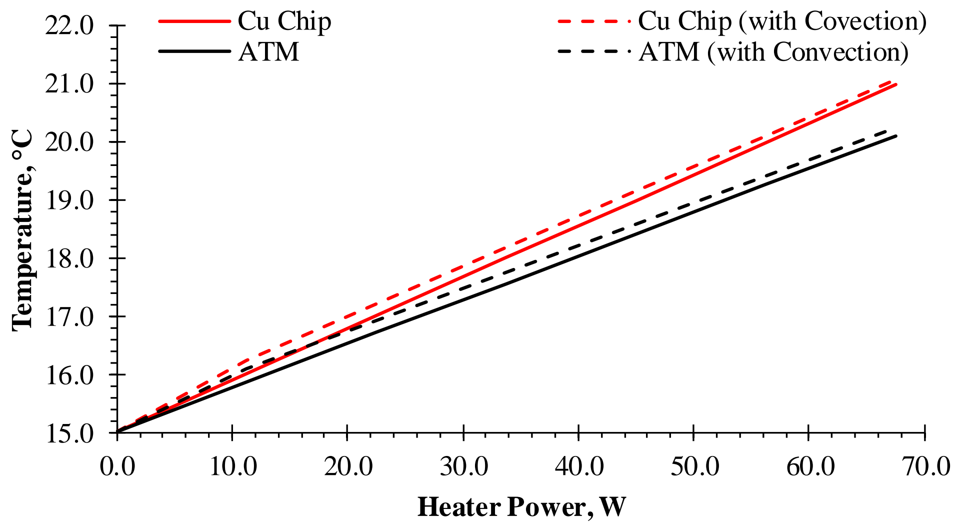

Figure 10. Convection Sensitivity Study

B. Preliminary Empirical Data

A simple test was conducted, with power applied to the X-Circuit and a thermocouple attached at the center of the bottom chip's circuit. The initial average temperatures converged to 17.5 °C, which was lower than predicted values at the applied power settings. This discrepancy may stem from systematic and statistical uncertainties in the power and temperature measurements.

The uncertainty in the power measurement to the circuit can be found by taking the partial derivative of Equation (6) with respect to current and resistance where we have systematic uncertainty. The partial derivatives provide the sensitivity of the system due to each input and are multiplied to by the corresponding systematic uncertainty. Power sensitivity is 11.24 W/A and 1600 W/Ω for current and resistance, respectively. The gauge error of the power supply

is ±0.005 A and gauge error for the resistance measurement is ±0.03 Ω. This results in a total uncertainty of the total power applied to the circuit of ±48.2 W. Therefore, the averaged pulsed power uncertainty is ±12.0 W.

Uncertainty due to the temperature measurements is comprised of statistical and systematic error. The temperature data acquisition device has a documented systematic error of ±0.9 °C based on the temperature readings and the rate of data acquisition. Based on the test data, the standard deviation was determined to be ±0.62 °C so the statistical uncertainty is ±1.24 °C for a 95% confidence interval. Therefore, the total uncertainty for the temperature is ±1.53 °C. Figure 10 shows the results of the average temperature and its associated errors plotted against the estimated temperatures provided by the model.

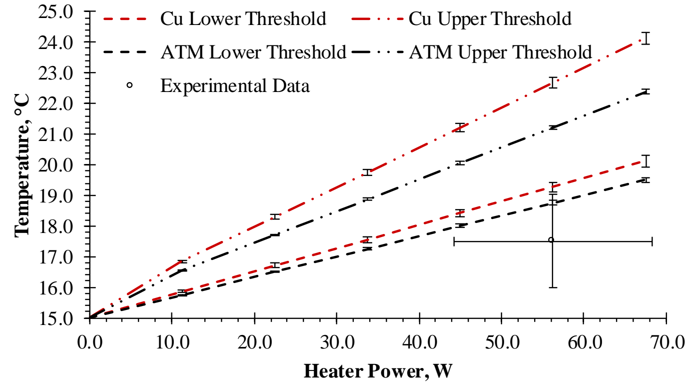

Figure 10. Preliminary Empirical Data

VI. Discussion and Conclusions

The results presented in the previous section show an ATM temperature reduction at a rate of 0.013 °C/W of applied power as compared to the original copper chip. Limited temperature reduction from the original chip to the AMT chip can be understood by simple one-dimensional resistance analysis. The equivalent resistance through the thickness of the material stack can be found by adding the thermal resistances in series, as if there were a point heat load and heat sink. The equivalent resistance along the length of the chips can also be calculated by adding the thermal resistances in parallel. By this simple approximation, the lateral thermal resistance is approximately 20 times that of the through-thicknes resistance for the original chip. This ratio is reduced to approximately 13 for the ATM chip. This implies that the increased lateral thermal conduction has a less significant impact on the temperature performance than do the through-thickness properties. This also accounts for the relatively large envelope found during a sensitivity study on through-thickness material parameters.

Although the model did not match the preliminary test results, it is apparent that the implementation of ATM technologies will improve the performance of the cold atom chip. Incorporating the ATM will provide cooler temperatures at a 0.013 °C/W rate, based on the change in temperature between the models and the change in power levels. The reduced temperature will allow for more power to be applied while maintaining atomic cloud generation capabilities.

The differences between the model results and the empirical data point can be due to several factors; the unmodeled prongs attached to the cold atom chip as shown in Figure 1, the thermal paste properties, imperfect knowledge of the physical workings of the cold atom chip, and poor experimental setup. The unmodeled prongs could potentially act as an unaccounted-for fin that will allow for energy to lost due to natural convection. This is compounded by the fact that this portion of the chip could potentially have the largest temperature gradient, as shown in Figure 5. Unfortunately, a thermocouple was not placed near this point, but this is an area of emphasis for future research. The thermal paste provided the most significant source of uncertainty with unknown thermal conductivity and thickness.

Continued research will further assist the characterization of the actual operating parameters of the chip-based cold atom INU. Testing the chips at different power levels while recording the temperatures with thermocouples and thermal imaging will provide targeted measurements at areas of interest and a more thorough depiction of the temperature gradient. These targeted empirical tests will potentially provide the data required to help reduce sources of uncertainty. Ultimately, empirical tests for the thermal response with ATM technologies incorporated into the INU system will be necessary to confirm the increased performance.

Acknowledgments

Funding for this work was performed under AFRL contract FA9453-17-C-0087 and FA9453-18-F-002. Many thanks go to the AFRL Cold Atom Chip team that presented this unique problem. Thanks go to AFRL and USRA for the opportunity to begin this work under the Summer Scholar program during the summer of 2017.

References

[1]K.M. Willis, "Signal Processing in Cold Atom Interferometry-Based INS", U.S. Air force Institute of Technology, Rept. AFIT-ENG-14-M-84, March 2014.

[2]R.A. Serway, *Physics For Scientist & Engineers with Modern Physics*, 3rd ed., Saunders College Publishing, Orlando, 1992, pp. 722.

[3]R. Chandratilleke, Y.Ohtani, H. Hatakeyama, H. Nakagome, "Development of Loop Heat Pipes for Cryogenic Applications", Sixteenth International Cryogenic Engineering Conference/International Cryogenic Materials Conference, 1997, pp. 501-504

[4]B.S. Taft, "Non-Condensable Gases and Oscillating Heat Pipe Operation," *Frontiers in Heat Pipes*, Vol. 4, No. 1, Global Digital Central, 2013.

[5]C. Wilson, B. Borgmeyer, R.A. Winholtz, H.B. Ma, D.L. Jacobson, D.S. Hussey, and M. Arif, "Visual Observation of Oscillating Heat Pipes Using Neutron Radiography," *Journal of Thermophysics and Heat Transfer*, Vol. 22, Iss. 3, The American Institute of Aeronautics and Astronautics, 2008, pp. 366-372.

[6]R.C. Givler and M.J. Martinez, "Modeling of Pulsating Heat Pipes," *Sandia Report SAND2009-4520*, Sanida National Laboratories, Albuquerque, NM, 2009.

[7]H.B. Ma, *Oscillating Heat Pipes*, Springer Science+Business Media, New York, 2015.

[8]"Advanced Solid Conduction: Improved Heat Spreading Efficiency in Action," https://www.thermacore.com/thermal-basics/advanced-solid-conduction.aspx#, Thermacore, accessed May 4, 2018.

[9]B.S. Taft, F.F. Laun, S.M. Smith, D.W. Hengeveld, Microgravity performance of a structurally embedded oscillating heat pipe, J. Thermophys. Heat Transfer 29 (2) (2015) 329–337.

[10]Irick, K. and Fathi, N., "Thermal Response of Open-Cell Porous Materials: A Numerical Study and Model Assessment," ASME 2018 Verification and Validation Symposium, American Society of Mechanical Engineers, New York, NY (submitted for publication).

[11]Celik, I. B., "Procedure for Estimation and Reporting of Uncertainty Due to Discretization in CFD Applications," Journal of Fluids Engineering, Vol. 130, Issue 7, ASME, 2008.

[12]Roache, P. J., *Fundamentals of Verification and Validation*, Hermosa Publishers, Socorro, NM, 2009

[13]Oberkampf, W. L. and Roy, C. J., Verification and Validation in Scientific Computing, Cambridge University Press, Cambridge, UK, 2010.

[14]C&R Technologies, *Thermal Desktop User Manual*, Software Package, Ver 5.8, Boulder, CO, 2015.